

Article

Comprehensive Thermal Modeling of ElectroThermoElastic Microstructures

Mohammad Mayyas

The University of Texas at Arlington Research Institute, Fort Worth, TX 76118, USA;
E-Mail: mmayyas@uta.edu; Tel.: +1-817-272-5887; Fax: +1-817-272-5952

*Received: 3 May 2012; in revised form: 16 August 2012 / Accepted: 17 August 2012 /
Published: 24 August 2012*

Abstract: Bent and folded beam configurations have been popularly used in electrothermoelastic (E-T) actuation. This paper introduces new designs of thermal end-effector with micro-grasping and micro-heating capabilities. We obtained analytical models for all possible steady state temperature responses of suspended and overhanging microstructures that constitute bent beam, folded beam, and combined actuators. Generally, the thermal response of E-T microstructures is sensitive to the boundary conditions, particularly for high power input. Thermal models have predicted the failure due to melting, which is the most common reason for failure of E-T devices, and it often occurs in the longest and the thinnest microstructure.

Keywords: electrothermal modeling; MEMS; micro grasper; end-effector

1. Introduction

Miniaturized end-effectors or “Microgrippers” located at the end of a robotic arm are primarily designed based on the complexity of the task for which the robot would be used. Different robotic actions that would require different designs include some fundamental manipulation processes such as grasping, placing, pushing, blowing, clamping, cutting, stapling and squeezing. In general, possible concept of end-effector can be obtained from passive and active structures that are designed to handle a set of tasks. In recent years, there is a growing demand to develop MicroElectroMechanical System (MEMS) end-effectors that are capable of handling and manipulating various micromponents for microassembly. Such MEMS structures could be potentially adapted for non-conventional endoscopic surgeries that require precision and delicate operations. Electrothermal (E-T) actuation based on

asymmetrical thermal expansion has popularly been applied to generate both the large force and deflection using structures such as bent beam and folded beam actuators [1–8].

Microstructures based on an array of thermal actuators provide powerful force and wide overall deflection [9–11]. A class of new active end-effectors based on an E-T actuation principle was introduced in our earlier work [7,11]. The performance of E-T actuators is limited by the maximum operating temperature and thermal stresses [12–14]. The coupling of “E-T to structural” is much stronger than the “structural to E-T” coupling. Thus, configuration and loading conditions of a micromachined material can independently determine the temperature profile at steady state.

E-T microstructures can be classified according to their release into three types [8]; overhanging (*released or totally exposed to ambient*), suspended (or the structure is separated *by an air gap from substrate*) and attached (or *physically attached to substrate*) microstructures. They can be fabricated from different materials using various technologies including Silicon on Insulator, SU8, and MUMPs [7]. The multi physics simulation of thermal MEMS actuators is often obtained from Finite Element Modeling (FEM) or Finite Element Approximation (FEA). Lerch *et al.* have studied the temperature distribution and deflection of a microstructure using a Finite Element (FE) analysis [12]. Lin and Chiao have used FE simulation to study the E-T response of a line-shape microstructure [8]. Mankame introduced a comprehensive thermal model for the FE simulation of E-T compliant structure [2]. However, analytical solutions provide more flexibility and physical insight, and facilitate a designer to explore additional constraints of failure, including potential melting which might be difficult to predict using FEA simulation due to the approximation algorithms used. Also, the analytical thermal models were previously obtained only for a few conditions focusing on low power E-T actuators.

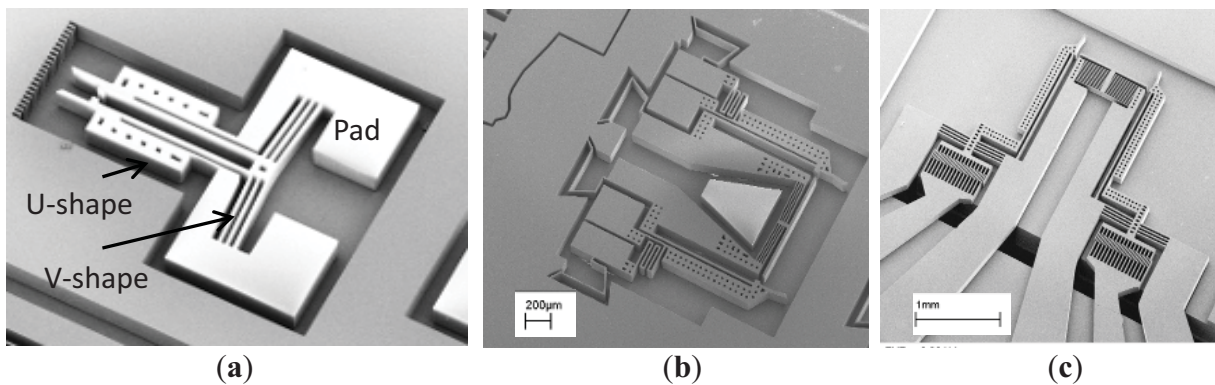
This paper presents comprehensive analytical E-T models that are obtained at a range of control input conditions for different ElectroThermoElastic microstructures. Temperature profiles at steady state of hanging and overhanging line-shape microstructures will be derived for layout combining bent and/or folded beams. Numerical simulations are obtained to support the analytical solutions. The structure of this paper is as follows: we start with practical examples of electrothermoelastic microstructures to motivate the reader with the possible application areas. Then, we introduce a reduced thermal model for the steady state heat conduction equation of a microstructure. Closed form expressions are obtained for configurations under several boundary conditions and power inputs, including suspended to overhanging microstructures. Finally, we compare the analytical solution with simulation results from finite element modeling and experimental findings.

2. Multipurpose Electrothermoelastic Microstructures

The integration of micro graspers and micros in single end-effector allow multiple or simultaneous processes to take place, such as assembly of micro parts and micro reflow based thermal bonding. Figure 1 shows examples of E-T actuators combining the performances of bent and folded beam microstructures, which are fabricated from homogenous material. The grasping or “opening and closing” mechanism is performed by a symmetric pair of E-T actuators acting in opposite directions. In general, grasping and heating incorporate two fundamental mechanisms: first a bent beam or (V-shape structure) whose apex moves forward due to the beam’s thermal expansion. An actuator comprising parallel bent beams could be either used to support large force gripping or to generate a

local heat flux at the interface of external micro-part. Second, the folded beam or (U-shape structure) asymmetrically expands to cause the grasper tip to bend in the direction of cold arm. The developed E-T end-effectors have two operational modes; active or passive grasping. The opening and closing in the active mode is controlled by an electrical signal. An input signal applied across the pad heats the resistive microstructure causing temperature to vary along the line-shape of the microstructure.

Figure 1. Examples of E-T end-effectors fabricated on Silicon On Insulator (SOI) material: (a) Micro grasper (combining bent-beam and folded-beam mechanisms) [7]. (b) The end-effector has grasper (obtained from folded beam mechanism), micro-heater (obtained from bent beam structure), and positioning sensor (obtained from resistive Zigzag structure); (c) A packaged end-effector incorporates multifunctional sensing and actuation capabilities.



On the other hand, V-shape actuators with parallel set of microbeams generate heat that can be possibly used in joining heterogeneous components for the constructing of microsystems. Similarly such structures could also be used for micro surgeries such as welding for presacral micro bleeding in a wound.

3. Steady-State Thermal Modeling

The microstructures could be fabricated from a single micromachined layer, and they can be modeled as a set of microbeams connected in series and/or parallel. In most fabricated MEMS actuators, microbeams are mostly rectangular bars of different widths and lengths and of uniform heights. The thermal response of (n) sequentially connected microbeams of different widths is sensitive to the air gap between the device and the substrate. Thus, the temperature profile along microbeams in an overhanging microstructure must be treated in a different way to those microstructures which are separated with air gaps.

In general, the temperature variation (T) along a microstructure (x) is governed by a nonlinear one dimensional Partial Differential Equation (PDE) with an input energy source from current (I) whose density along microbeam is ($J = I/wh$) [6,7,13]. A suspended rectangular bar with width w and height (h) is kept at a fixed air gap distance relative to the substrate. The rate of heat change per unit area is equal to the heat production per unit volume ($A \cdot dx$) per time minus heat losses, or [7]

$$\rho_d C_p \frac{\partial T}{\partial t} dx = \left(\frac{I}{wh} \right)^2 \rho_r dx - \left[\frac{d}{dx} \left(-k_p \frac{dT}{dx} \right) dx + (T - T_p) \left(\frac{S}{hR_T} \right) dx + \left(\frac{2h_{cs}}{w} + \frac{\lambda h_{cf}}{h} \right) (T - T_a) dx + \frac{\lambda \epsilon_e \sigma}{h} (T^4 - T_b^4) dx \right] \quad (1)$$

Equation (1) is a general 1-D transient heat conduction that combines the nonlinearity of heat conduction coefficient and the effect of radiation heat transfer. Convection coefficients (h_{cs}) and h_{cu} correspond to the thermal convection heat losses off the side wall and the faces of microbeams, respectively. λ is a numeric factor introduced here to describe the heat loss condition. (λ) is equal to one when heat conduction through air gap is considered. However, (λ) is two when microbeams are experiencing convection from all sides with no conduction to other layers, *i.e.*, shape factor (S) is zero. ρ_d and C_p are material density and specific heat of actuator, respectively. The resistivity of microbeam (ρ_r) is linearly dependent on temperature. The thermal conductivity of the actuator material ($k_p(T)$) will be later assumed constant. (T_p , T_a and T_b) are constant temperatures of the bottom surface of the substrate, ambient and of a black body, respectively. All are assumed here to be equal to some constant temperature (T_s). The nonlinear radiation term in Equation (1) is proportional to Stefan-Boltzmann constant (σ) and micro-surface emissivity (ε_e).

The shape factors of the heat conduction (S) impacts the shape of the element on the excessive heat conduction to the substrate [8]. A shape factor is defined by the total heat flux out of the line-shape microbeam per unit length divided by heat flux going directly under the width of a microbeam [6,8,15]. It is given by

$$S = \frac{h}{w} \left(\frac{2t_v}{h} + 1 \right) + 1 \quad (2)$$

Few micrometer of air gap can be modeled as a conductive layer with zero Young's Modulus and infinite electrical resistivity. (R_T) is a thermal resistance between the thermal microbeam and the substrate. For microbeam suspended on two sandwiched layers, such as SOI, the thermal resistance is

$$R_T = \frac{t_v}{k_v} + \frac{t_s}{k_s} \quad (3)$$

where (t_v) and (t_s) are the air gap and substrate thicknesses, respectively. (k_v) and (k_s) are the thermal conductivity of the air and a substrate, respectively.

The electrical resistivity of microbeam is function of its temperature, and it is assumed to have a linear thermal coefficient (ξ), that is

$$\rho_r(T) = \rho_o \left[1 + \xi (T - T_p) \right] \quad (4)$$

Thermal conductivity (k_p) of silicon is generally dependent on temperature variation. It is generally approximated in a third order polynomial [16]

$$k_p = \psi_o + \psi_1 T + \psi_2 T^2 + \psi_3 T^3 \quad (5)$$

where the non-constant terms add non linearity to the governing equation making the conductive structure to have higher and more sensitivity for temperature change.

Surface heat radiation by convection and radiation in small structures should be considered at high operating temperature, normally above 500 K [2]. The radiation heat transfer is significant in suspended or separated structures which are experiencing high temperature difference at small gaps range between 1–10 μm [8,17]. To simplify Equation (1), the radiation term is dropped. Thermal conductivity is assumed to be temperature independent. The Steady State Heat Equation is obtained by dropping the time partial derivative in Equation (1) and reduces into second order ODE Equation (6a).

The Eigen values of its characteristic equation determine the solution profile. In general, for n serially connected microbeams, the temperature profile is determined by the flowing critical current ($I_{(i)}$ or $\beta_{(i)}$) value, and it is obtained from the roots of the characteristic equation of the ODE

$$k_p \frac{d^2T}{dx^2} - \left(\frac{2h_{cs}}{h} + \frac{\lambda h_{cf}}{h} + \frac{S}{hR_T} - \rho_o \xi \right) T(x) + \left[\left(\frac{I}{wh} \right)^2 [\rho_o - \xi T_p] + \frac{T_p S}{hR_T} + T_a \left(\frac{2h_{cs}}{w} + \frac{\lambda h_{cf}}{h} \right) \right] \quad (6a)$$

After arranging the eigenvalues and substituting Equations (2), (3), (5) in Equation (6a), we get

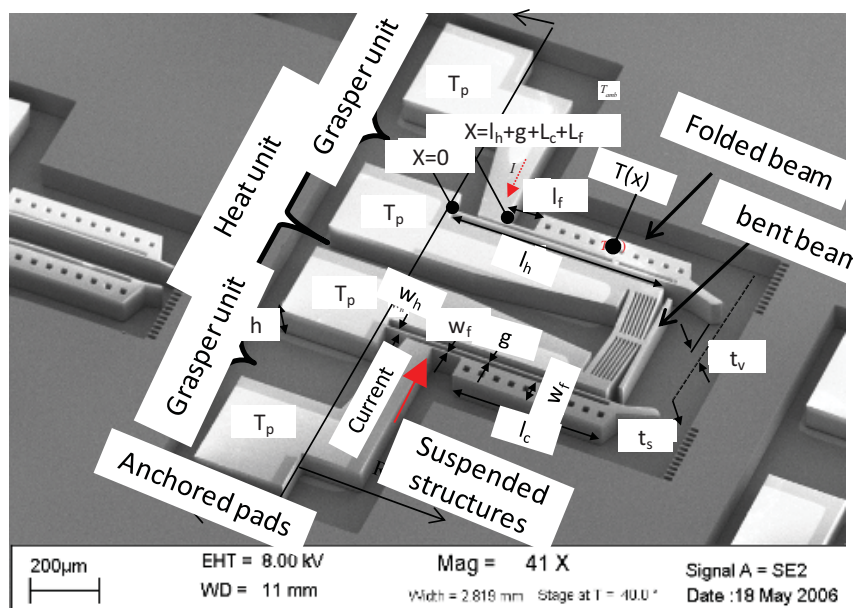
$$\left\{ \begin{aligned} I_{(i)} &= \sqrt{\frac{k_v k_s \xi_{(i)} w_{(i)} \rho_o (2t_v + h + w_{(i)}) + (k_v t_s + k_s t_v) (w_{(i)} \lambda h_{cf(i)} + 2h h_{cs(i)})}{\xi_{(i)} h \rho_o (k_v t_s + k_s t_v)}} \\ \text{or} \\ \beta_{(i)} &= \left(\frac{S_i}{hR_T} + w_i \lambda h_{cf(i)} + 2h h_{cs(i)} - J_{(i)}^2 \rho_o \xi_{(i)} \right) \end{aligned} \right. \quad i = 1, \dots, n \quad (6b)$$

This criterion is a property of a microstructure that determines the temperature profile when compared to the current flow I . The subscript (i) refers to the beam number or name in n -serially connected beams.

3.1. Folded or Bent Beam E-T Actuators

A single layer folded beam actuator in Figure 2 has three serially connected micobeams ($n = 3$). Its temperature distribution ($T(x)$) is continuous; starts from an anchored pad at ($x = 0$), passes through a hot arm (*subscript h*), then through cold arm (*subscript c*), then flexure arm (*subscript f*), and ends up to another anchored pad at ($x = l_h + g + l_c + l_f$). The total number of boundary conditions needed to solve the unknown constants is $2n$.

Figure 2. The E-T actuator comprises a grasping mechanism and a heating element.



Case 1. Suspended microstructures with exponential profiles when (I_h, I_c and $I_f < I$)

The exponential temperature profiles, which normally take place at considerably low input voltage, have been discussed before and will be reviewed in this paper for completeness [14]. The temperature profile along the microbeams is defined by an exponential function given that ($\beta_h, \beta_c, \beta_f > 0$); i.e., the input current is greater than the right hand side in Equation (6) or (I_h, I_c and $I_f < 1$). The line-shape temperature profiles along each beam is

$$T_i(x_i) = T_{\infty i} + C_{1i}e^{\sqrt{\frac{\beta_i}{\psi_o}}x_i} + C_{2i}e^{-\sqrt{\frac{\beta_i}{\psi_o}}x_i}, \quad i = h, c, f \tag{7}$$

where $T_{\infty i} = (T_p + J_i^2 \rho_0 / \beta_i)$. The temperature profile along the three connected microbeams is continuous. The unknown are solved from the continuity of temperature profile and heat flow. Applying the boundary conditions into the Steady State Heat Conduction Equation (SSHCE) gives the unknown constants (C_{ij})

$$\begin{bmatrix} C_{1h} \\ C_{2h} \\ C_{1c} \\ C_{2c} \\ C_{1f} \\ C_{2f} \end{bmatrix} = \begin{bmatrix} 1 & 1 & 0 & 0 & 0 & 0 \\ e^{\sqrt{\frac{\beta_h}{\psi_o}}(L+g)} & e^{-\sqrt{\frac{\beta_h}{\psi_o}}(L+g)} & -e^{\sqrt{\frac{\beta_c}{\psi_o}}(L+g)} & -e^{-\sqrt{\frac{\beta_c}{\psi_o}}(L+g)} & 0 & 0 \\ e^{\sqrt{\frac{\beta_h}{\psi_o}}(L+g)} & -e^{-\sqrt{\frac{\beta_h}{\psi_o}}(L+g)} & -\frac{w_c}{w_h} \sqrt{\frac{\beta_c}{\psi_o}} e^{\sqrt{\frac{\beta_c}{\psi_o}}(L+g)} & \frac{w_c}{w_h} \sqrt{\frac{\beta_c}{\psi_o}} e^{-\sqrt{\frac{\beta_c}{\psi_o}}(L+g)} & 0 & 0 \\ 0 & 0 & e^{\sqrt{\frac{\beta_f}{\psi_o}}(L+g+L_c)} & e^{-\sqrt{\frac{\beta_f}{\psi_o}}(L+g+L_c)} & -e^{\sqrt{\frac{\beta_f}{\psi_o}}(L+g+L_c)} & -e^{-\sqrt{\frac{\beta_f}{\psi_o}}(L+g+L_c)} \\ 0 & 0 & e^{\sqrt{\frac{\beta_f}{\psi_o}}(L+g+L_c)} & -e^{-\sqrt{\frac{\beta_f}{\psi_o}}(L+g+L_c)} & -\frac{w_f}{w_c} \sqrt{\frac{\beta_f}{\psi_o}} e^{\sqrt{\frac{\beta_f}{\psi_o}}(L+g+L_c)} & \frac{w_f}{w_c} \sqrt{\frac{\beta_f}{\psi_o}} e^{-\sqrt{\frac{\beta_f}{\psi_o}}(L+g+L_c)} \\ 0 & 0 & 0 & 0 & e^{\sqrt{\frac{\beta_f}{\psi_o}}(2L+g)} & e^{-\sqrt{\frac{\beta_f}{\psi_o}}(2L+g)} \end{bmatrix} \begin{bmatrix} T_s - T_{\infty h} \\ T_{\infty c} - T_{\infty h} \\ 0 \\ T_{\infty f} - T_{\infty c} \\ 0 \\ T_s - T_{\infty f} \end{bmatrix} \tag{8}$$

Case 2. Suspended microstructures with mixed profiles when ($I_h, I_f < I$ and $I_c > I$)

Mixed temperature profiles normally take place when the width of a cold arm in a folded beam actuator is larger than that of hot and flexure arms. This causes the exponential thermal responses in the hot and flexure arms to drift into a sinusoidal profile as the input current increases beyond the critical values. When ($\beta_h, \beta_f < 0$ and $\beta_c > 0$), the temperature profiles of hot and flexure arms are given by

$$T_i(x_i) = T_{\infty i} + C_{1i} \cos\left(\sqrt{\frac{|\beta_i|}{\psi_o}}x_i\right) + C_{2i} \sin\left(\sqrt{\frac{|\beta_i|}{\psi_o}}x_i\right) \quad i = h, f$$

$$T_c(x_c) = T_{\infty c} + C_{1c}e^{\sqrt{\frac{\beta_c}{\psi_o}}x_c} + C_{2c}e^{-\sqrt{\frac{\beta_c}{\psi_o}}x_c} \tag{9}$$

Case 3. Suspended microstructures with sinusoidal profiles when (I_h, I_c and $I_f > I$)

Sinusoidal response in all of the serially connected microbeams generally occurs at high input current. When ($\beta_h, \beta_c, \beta_f < 0$) becomes true, the solution becomes

$$T_i(x_i) = T_{\infty i} + C_{1i} \cos\left(\sqrt{\frac{|\beta_i|}{\psi_o}}x_i\right) + C_{2i} \sin\left(\sqrt{\frac{|\beta_i|}{\psi_o}}x_i\right) \quad , i = h, c, f \tag{10}$$

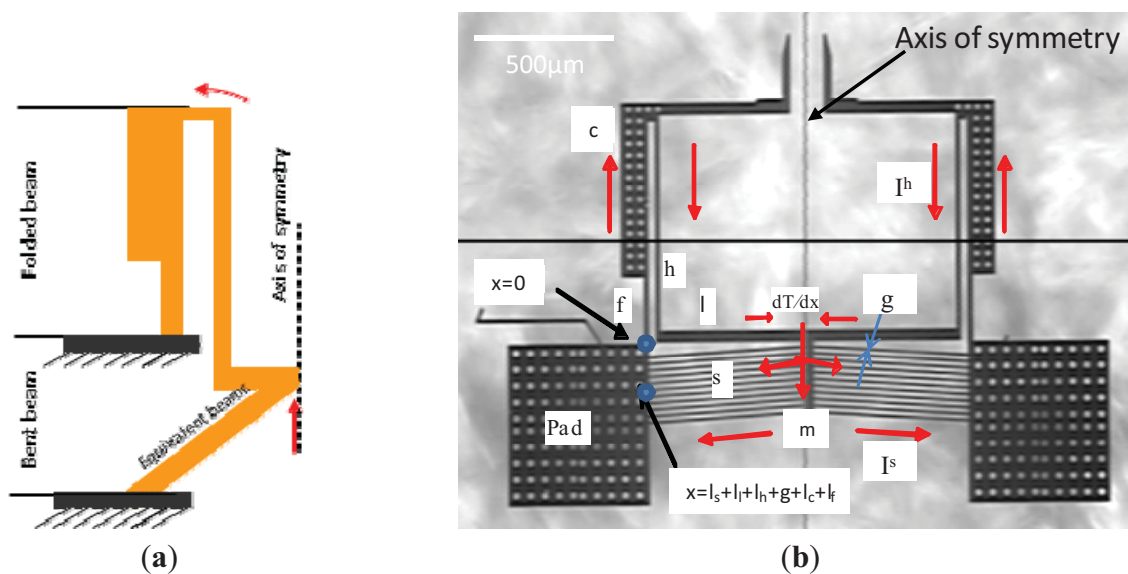
The ‘‘bent beam’’ model can be obtained from ‘‘folded beam’’ model with uniform width of w_u . Where the equations derived in the above three cases can be used for ‘‘bent beam’’ given that

$w_u = w_h = w_c = w_f$. For microbeams of the same width, the critical condition $\beta_h, \beta_c, \beta_f = 0$ gives constant temperature profile $T_h(x) = T_c(x) = T_f(x) = T_p$. In this case, the amount of heat generation is equal to the amount of heat lost across a substrate. There are only two cases in “bent beam” microstructures: (i) exponential profile which corresponds to low temperature; or (ii) sinusoidal profile pertaining high temperature response.

3.2. Combined Bent and Folded Beam Actuator

A different class of E-T actuator is obtained when the performances of the bent and folded beam are combined in a single microstructure. The grasper in Figure 3 has two symmetrical structures with each having a series of connected microbeams. Each side starts from an anchored pad at ($x = 0$), passes through bent beams (*subscript s*), then a linkage arm (*subscript l*), then a hot arm (*subscript h*), then through a cold arm (*subscript c*), then a flexure arm (*subscript f*), and ends up to same anchored pad at ($x = l_s + l_l + l_h + g + l_c + l_f$). The (g) is the gap between the hot and cold arm. The current density across the hot arm, linkage arm, and bent beam causes high thermal expansion as compared to cold arm. Concurrently, the bent beams push the linkage arm forward. Thus, each tip in the grasper bends toward the cold arm with a greater overall all “opening and closing”.

Figure 3. Micro grasper combining folded and bent beam mechanisms: (a) sketch; (b) E-T actuator fabricated from SOI.



For this class of E-T actuator, the symmetry in the structure and the boundary conditions yield symmetrical temperature distribution about the “Axis of symmetry”, indicated in Figure 3. The structure across this line is adiabatic where the temperature is at least local maximum. The temperature distribution along beams can be linearly solved in a line shape starting from one pad and ending at the same pad. The temperature’s drop due to the “middle link (m)” electrical resistance could be neglected because the beam has short length. Thus, the temperatures difference across a parallel set of bent beams is assumed unchanged. It is sufficient to solve for temperature profile about one side of axis of thermal symmetry. The following cases are analogous to the previous discussion:

Case 1. Suspended microstructure with exponential profiles ($I_f, I_c, I_h, I_l, I_s < I$)

We consider E-T actuator whose device structure is suspended with an air gap separating it from the substrate. The temperature profile of a microstructure is governed by exponential steady state when ($\beta_f, \beta_c, \beta_h, \beta_l, \beta_s > 0$) is hold. The temperature profile along microbeams is continuous, start from pad temperatures at a flexure arm and end up with same pad temperature at the end of bent beams. The temperature profiles are

$$T_i(x) = T_{\infty i} + C_{1i}e^{\sqrt{\frac{\beta_i}{\psi_o}}x} + C_{2i}e^{-\sqrt{\frac{\beta_i}{\psi_o}}x}, \quad i = f, c, h, l, s \tag{11}$$

The current passing through each beam is extracted from circuit analogy network. The current passing through the “folded beam” including flexure, cold, hot and linkage arm is

$$I^h = \frac{IR_s}{(R_h + R_s)} \tag{12}$$

(R_s) and (R_h) are the overall electrical resistance of folded and bent beams in the microstructure, respectively. I is the total current drawn across the pad due to overall resistance, where $I = I^h + I^s$ and I^s is the current passing in each one of the (q) bent beams

$$I^s = \frac{IR_h}{q(R_h + R_s)} \tag{13}$$

The electrical resistances are temperature dependent and their average can be simplified into

$$R_h = \int_0^{l_f+l_c+l_g+l_l} dR(T) = \frac{l_f}{w_f h} \rho_o (1 + \xi(\bar{T}_f - T_s)) + \frac{l_c}{w_c h} \rho_o (1 + \xi(\bar{T}_c - T_s)) + \frac{l_h+g}{w_h h} \rho_o (1 + \xi(\bar{T}_h - T_s)) + \frac{l_l}{w_l h} \rho_o (1 + \xi(\bar{T}_l - T_s))$$

$$R_s = \frac{1}{q} \int_{l_f+l_c+l_g+l_l}^{l_f+l_c+l_g+l_l+l_s} dR(T) = \frac{l_s}{q w_s h} \rho_o (1 + \xi(\bar{T}_s - T_s)).$$
(14)

Thus, the voltage across the pads is

$$V = \frac{2I(R_s R_h)}{R_s + R_h} \tag{15}$$

Alternatively, the resistances could be estimated from resistivity calculated at some close average temperature (ρ_a)

$$R_h = \frac{\rho_a}{h} \left(\frac{l_f}{w_f} + \frac{l_c}{w_c} + \frac{l_h}{w_h} + \frac{l_l}{w_l} \right), \text{ and } R_s = \rho_a \frac{l_s}{q h w_s} \tag{16}$$

Case 2. Overhanging microstructure operating on ambient

The previous equation from Case 1 is valid for overhanging E-T actuators. The heat is lost to the ambient through natural convection, and the given the following criterion hold

$$\beta_i = \left(\left(\frac{2h_{csi}}{w_i} + \frac{\lambda h_{cfi}}{h} \right) - J_i^2 \rho_o \xi \right) > 0 \quad i = f, c, h, l, s \tag{17}$$

This case is equivalent to the suspended E-T actuators which is described in Case 1 of Section 3.1, but with large air gap, *i.e.*, the structure becomes overhanging. In such cases Equation (6b) can be replaced by Equation (17).

Case 3. Sinusoidal profiles

Temperature proliferates along structures in wavy profile. This occurs when one or both of the heat losses (*conduction through substrate or/and convection to ambient*) are relatively lower than the generated heat. Subcases includes first, both suspended and overhanging microstructures in Cases 2 and 3 are operating at relatively high input current such that $\{\beta_i < 0, \forall i = f, c, h, l, s\}$. Second, E-T actuators is operating in vacuum with no heat losses where $\beta_i = J_i^2 \rho \zeta$ and $T_{\infty i} = T - 1/\zeta$.

The governing equations yield sinusoidal profiles along all microstructures

$$T_i(x) = \alpha_i + C_{1i} \sin \sqrt{\frac{\beta_i}{\psi_o}} + C_{2i} \cos \sqrt{\frac{\beta_i}{\psi_o}} \quad i = f, c, h, l, s \quad (18)$$

Other cases might be obtained for mid-range input power, where the profiles combine exponential and sinusoidal shapes.

4. Simulation and Experimental Results

Finite Difference Method (FDA) and Finite Element Modeling (FEM) are compared with the exact solutions at different power input and boundary conditions. The FDA simulation is used to verify the mathematics of the exact expression with some degree of proximity. But it does not validate the exactness of the physical model. In FDA, the general solution of a rising temperature distribution could be obtained by Forward-Time Centered- Space method (FTCS). For E-T actuators with n -serially connected microstructures, the FDA of Equation (1) without heat radiation term can be written in a discrete format

$$T_{\chi}^{\omega+1} = \left(\frac{{}^i\alpha_p \Delta t}{\Delta x^2} \right) \left(T_{\chi-1}^{\omega} - T_{\chi}^{\omega} \left(2 + {}^i\varepsilon \Delta x^2 - \frac{\Delta x^2}{{}^i\alpha_p \Delta t} \right) + T_{\chi+1}^{\omega} + {}^i T_{\infty}^i \varepsilon \Delta x^2 \right), i = 1, \dots, n \quad (19)$$

where ($\varepsilon = \beta/\psi_o$, $\varepsilon > 0$), (ω) and (χ) are integers that refer to the time and the space mesh, respectively. (Δx) and (Δt) are space and time grid resolution, respectively. Equation (19) is a general equation which can solve for any serially connected microstructures. The intermediate B.C's between different microbeams are automatically embedded in the formula. Also, it can handle non-homogenous material and thickness properties across different microbeams. When an m parallel network of microbeam is introduced, a set of m n -serially connected equations must be solved simultaneously for the unknowns.

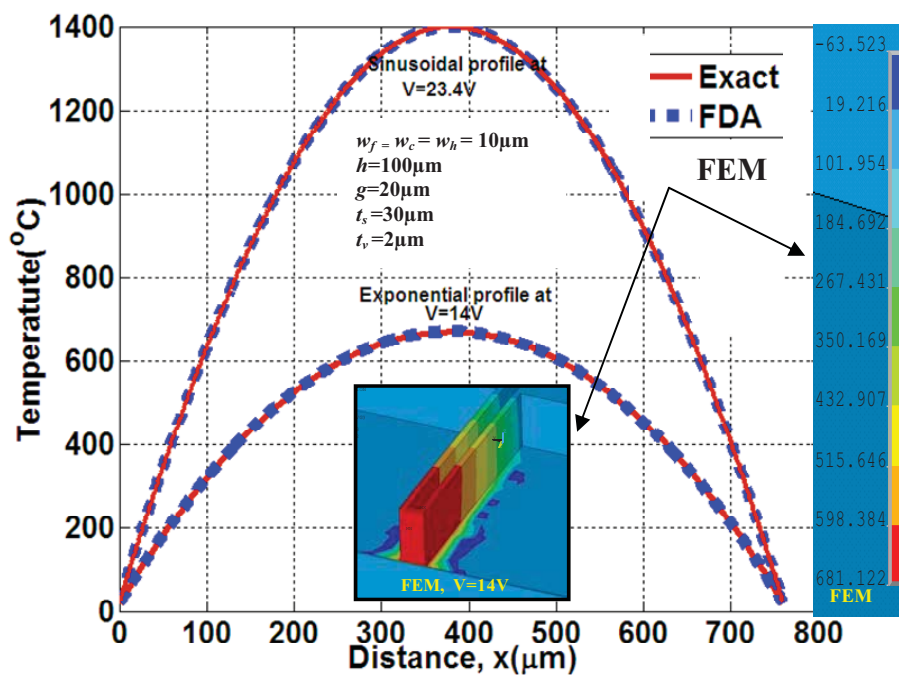
A physical model of a bent beam E-T actuator is used for comparison. The model is obtained for device layer fabricated on silicon substrate by deep reactive ion etching (DRIE) process on SOI wafers. The material properties and dimensions for a uniform width device layer are indicated in Table 1, and listed in Figure 4, respectively. The steady state temperature profiles for a single suspended bent beam E-T actuator are obtained from FEM, FDA and analytical model. FEM result is obtained from tetrahedral elements with polynomial based on second order expansion series. FEM and FDA are compared against analytical model for low and high power input. In the low power input, the exponential profile preserves the shape until 14 V. As the voltage increases the profile smoothly

switches into sinusoidal keeping same profile shape. In both cases, the profiles maintain one local maximum at the beam center as indicated in Figure 4. The FDA, FEM and Exact methods are all in good agreement for low and medium power input magnitude.

Table 1. Material properties of SOI actuators.

SOI Layers Parameter	Si Device	Si wafer substrate	Air
Density, ρ_d (Kg/m ³)	2,330	2,330	0.524
Thermal conductivity, (Wm ⁻¹ °C ⁻¹)	100	30	3.37×10^{-2}
Thermal Expansion, α ($10^{-6} \times$ °C ⁻¹)	3.1	3.1	1.49×10^3
Thermal Capacity, C_p (J·Kg ⁻¹ ·°C ⁻¹)	787	787	1,013
Temperature coefficient, ζ ($10^{-3} \times$ °C ⁻¹)	1.25	1.25	-
Electrical resistivity, ρ_o (Ω ·m)	1.51×10^{-4}	2.5×10^{-2}	3×10^{13}
Modulus of Elasticity, E (GPa)	169	169	-
Poison ratio, ν	0.22	0.22	-

Figure 4. Simulations of the temperature profile in a single bent beam.



The steady state temperature profiles in of suspended folded beam actuator are simulated under no heat convection. The material properties and dimensions for a uniform width device layer are indicated in Table 1, and listed in Figure 5, respectively. Figure 5 shows variation of temperature profile along beams. At low input power (6.8 V), the steady-state temperatures in all beams are exponential. Increasing the input power up to 10 V has brought temperature response in thin-beams into sinusoidal. On the other hand, increasing the power input induces higher frequencies with multiple peaks across the microstructure. This type of response might be experimentally observed if the temperature-peaks do not exceed the melting point of the structure. It is worth to mention here that the approximation nature in finite element or finite difference element might not be sufficient to capture high temperature-peak fluctuation along microstructures.

Figure 5. Simulations of the temperature profile in folded beam actuator.

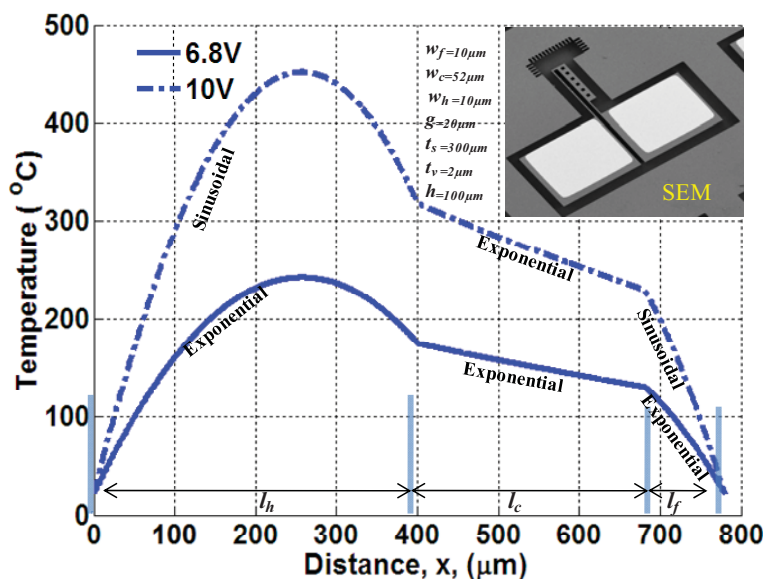
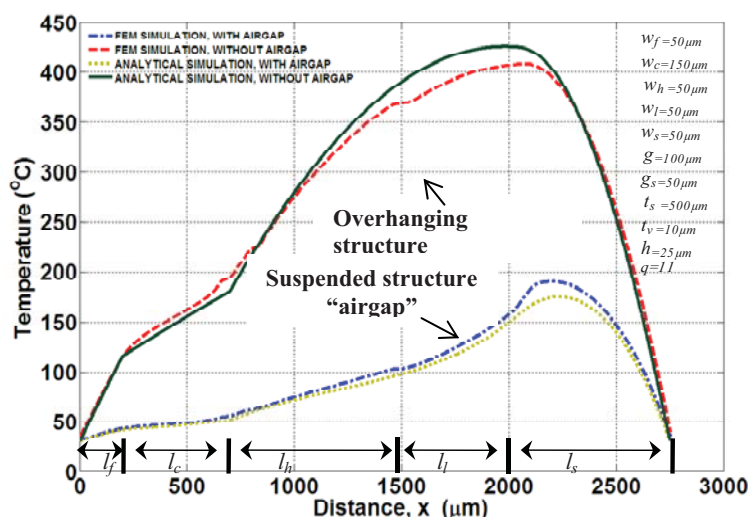


Figure 6. Simulations of combined bent and folded beam actuator.



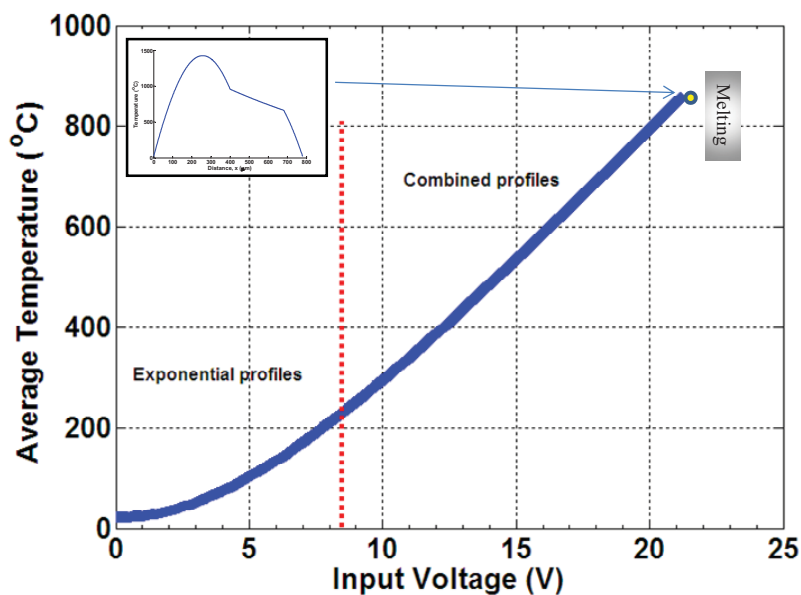
Examples on the steady state temperature profile of “combined bent beam and folded beams” are simulated for two types of actuators: overhanging and suspended structure similar to configuration in Figure 3. The simulations are obtained at low power input of 1 V and at vacuum condition, *i.e.*, without heat convection. Figure 6 shows the trend of the temperature profile which starts from flexure and ends up at the bent beam. The local maximum temperature is often located at the adiabatic line where the bent beams are connected to the linkage arm. The temperature profiles of suspended actuator have exponential responses along the entire microstructures. This is due to considerable heat loss through the conductive air gap. More increase in the air gap decreases heat loss and may bring the condition in Case 1 into either Case 2 or 3 as described in Section 3.2. When the air gap is relatively large, the actuator becomes completely governed by sinusoidal profiles with significant increase in temperatures magnitude. We also notice that there is a slight difference between FEM and analytical result. One reason might be related to the averaging of thermal resistance. This has also led to a clear temperature difference between FEM and analytical around adiabatic line.

The continuity of the analytical models about the critical currents can be checked from the continuity of the average temperature over a range of input power. The overall average temperature for n -serially connected microbeams, whose length (l_k) and temperature profile ($T_k(x)$, $l_k \geq x \geq l_{k-1}$), can be lumped into

$$\bar{T} = \sum_{k=1}^n \left(l_k T_{\text{avg}k} + \int_{l_{k-1}}^{l_k} T_k(x) dx \right) / \sum_{k=1}^n l_k \quad (20)$$

Figure 7 describes the continuity of temperature profiles over a range of input power for the dimension and materials in Figure 5 and Table 1, respectively. The simulation is stopped at average of ~ 860 °C where the material hypothetically fails due to melting (1,414 °C for silicon).

Figure 7. Simulation of \bar{T} in folded beam from analytical models.



At about 8.3 V input, the average temperature is piece-wise smooth. The temperature profiles along the microstructures start to change from “exponential profiles” into “mixed profiles”, where the hot and flexure arms experience sinusoidal profiles while the cold arm maintains an exponential profile.

One useful application of the analytical expression is to understand thermal failure. For example, the hot-arm of folded beam E-T actuator in Figure 5 glows as the power input gets closer to 14 V. Multiple types of structural/thermal failure were captured. FEM and digital image of thermal failure are utilized to differentiate between the stress and melting failures.

In Figure 8, the Von-Mises thermal stress and temperature distribution were simulated along the microstructures for inputs 14.5 V and 20 V. The silicon compressive strength is 120 MPa [13]. The dimensions and properties for the FEM simulation are from Figure 5, and Table 1, respectively. The FEM analysis suggests that the thermal stress at 14.5 V may not cause failure at root of flexure arm. However, the melting occurred in the “hot arm” microbeam with a peak temperature of 1,414 °C, as shown Figure 9(b). On the other hand, the folded beam in Figure 9(c) has two distinct failures caused by input of 20 V: the first is melting failure due to maximum temperature at hot arm, and the second is thermo structural failures due to stresses around the roots of flexure and hot arms.

Figure 8. Thermal stress and temperature distribution of folded beam actuator.

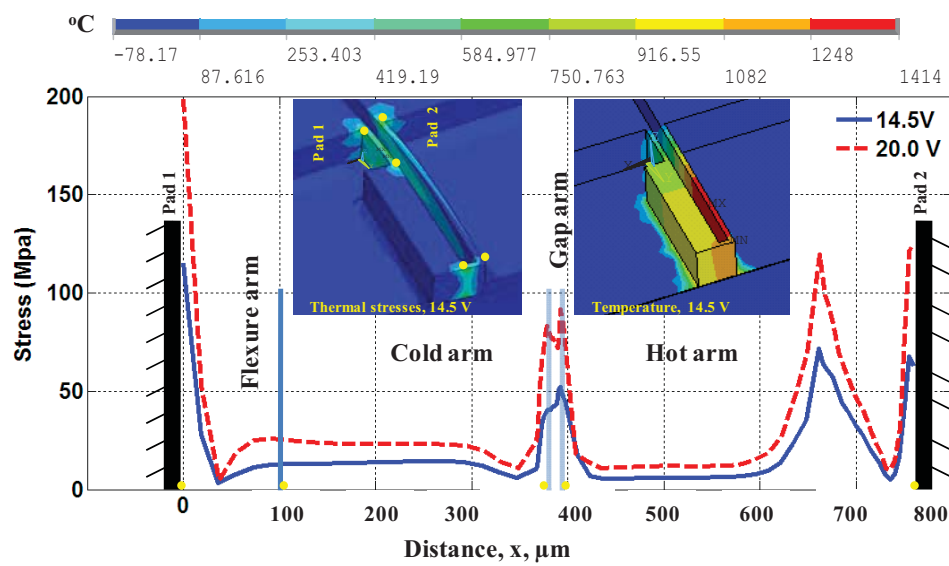
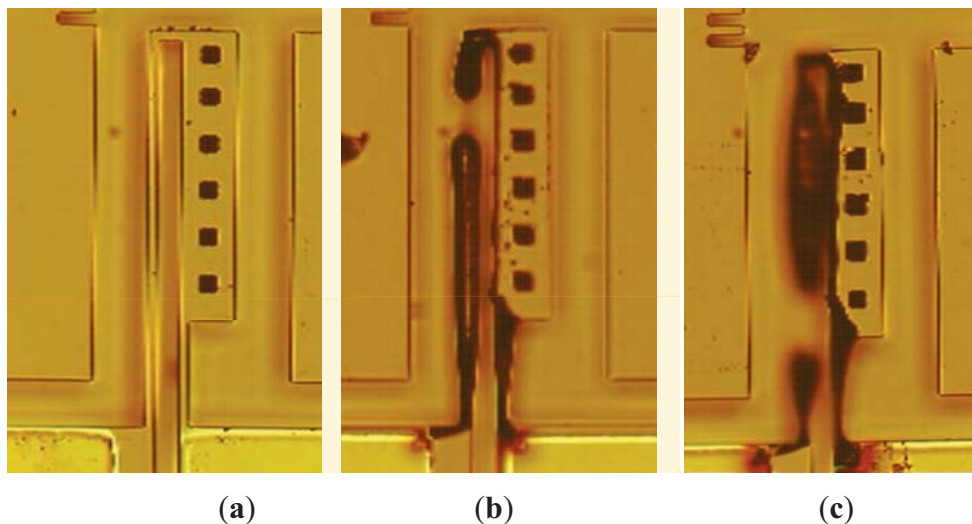


Figure 9. Thermal failure experiments: (a) SOI folded beam; (b) failure on hot arm due to melting at (~14.4 V); (c) multi failures in hot and flexure arms due to (~20 V).



5. Conclusions

Reduced order electrothermal models of suspended and overhanging microstructures are introduced for several configurations: (i) folded beams, (ii) bent beam, and (iii) combined shape from bent and folded beam. The analytical solutions are in good agreement with the FEM model, particularly when the temperature profile is relatively low. E-T actuators which operate in ambient temperatures often undergo sinusoidal temperature response that requires thermal management due to low heat dissipation. Microstructures which are separated by small air gaps from a heat sink often undergo exponential temperature response at low power input into sinusoidal or mixed temperature responses at higher power input. The sensitivity of the temperature response due to the change in the power is higher in sinusoidal than exponential response. Future work includes thermo-elastic modeling of combined shape actuator.

References

1. Luo, J.K.; Flewitt, A.J.; Spearing, S.M.; Fleck, N.A. Comparison of microtweezers based on three lateral thermal actuator configurations. *J. Micromech. Microeng.* **2005**, *15*, 1294–1302.
2. Mankame, N.D.; Ananthasuresh, G.K. Comprehensive thermal modeling and characterization of an electro-thermal-compliant microactuator. *J. Micromech. Microeng.* **2001**, *11*, 452–462.
3. Riethmuller, W.; Benecke, W. Thermally excited silicon microactuators. *IEEE Trans. Electron. Devices* **1988**, *35*, 758–763.
4. Pany, C.; Hsu, W. An electro-thermally and laterally driven polysilicon microactuator. *J. Micromech. Microeng.* **1997**, *7*, 7–13.
5. Field, L.A.; Burriesci, D.L.; Robrish, P.R.; Ruby, R.C. Micromachined 1×2 optical-fiber switch. *Sens. Actuators A* **1996**, *53*, 311–315.
6. Huang, Q.-A.; Ka, N.; Lee, S. Analysis and design of polysilicon thermal flexure actuator. *J. Micromech. Microeng.* **1999**, *9*, 64–70.
7. Mayyas, M.; Stephanou, H. Electrothermoelastic modeling of MEMS gripper. *Microsyst. Technol.* **2009**, *15*, 637–646.
8. Lin, L.W.; Chiao, M. Electrothermal responses of lineshape microstructures. *Sens. Actuators A* **1996**, *55*, 35–41.
9. Lee, W.H.; Kang, B.H.; Oh, Y.S.; Stephanou, H.; Sanderson, A.C.; Skidmore, G.; Ellis, M. Micropeg Manipulation with a Compliant Microgripper. In *Proceedings of IEEE International Conference on Robotics and Automation*, Taipei, Taiwan, 14–19 September 2003; pp. 3213–3218.
10. Mayyas, M.; Shiakolas, P.S.; Lee, W.H.; Popa, D.; Stephanou, H. Static and Dynamic Modeling of Thermal Microgripper. In *Proceedings of the 14th Mediterranean Conference on Control and Automation (MED '06)*, Ancona, Italy, 28–30 June 2006.
11. Mayyas, M.; Zhang, P.; Lee, W.H.; Shiakolas, P.; Popa, D. Design Tradeoffs for Electrothermal Microgrippers. In *Proceedings of IEEE International Conference on Robotics and Automation*, Roma, Italy, 10–14 April 2007.
12. Lerch, P.; Slimane, C.K.; Romanowicz, B.; Renaud, P. Modelization and characterization of asymmetrical thermal microactuators. *J. Micromech. Microeng.* **1996**, *6*, 134–137.
13. Mayyas, M.; Shiakolas, P. A Study on the Thermal Behavior of Electrothermal Microactuators Due to Various Voltage Inputs. In *Proceedings of ASME IMECE*, IMECE2006-15321, Chicago, IL, USA, 5–10 November 2006.
14. Butler, J.T.; Bright, V.M.; Cowan, W.D. Average power control and positioning of polysilicon thermal actuators. *Sens. Actuators* **1999**, *72*, 88–97.
15. Brnas, D.M.; Bright, V.M. Design and performance of a double hot arm polysilicon thermal actuator. *Proc. SPIE* **1997**, *3224*, 296–306.
16. Uma, S.; McConnell, A.D.; Asheghi, M.; Kurabayashi, K.; Goodson, K.E. Temperature-dependent thermal conductivity of undoped polycrystalline silicon layers. *Int. J. Thermophys.* **2001**, *22*, doi:10.1023/A:1010791302387.

17. Polder, D.; Hove, M.V. Theory of radiative heat transfer between closely spaced bodies. *Phys. Rev. B* **1971**, *4*, 3303–3314.

© 2012 by the authors; licensee MDPI, Basel, Switzerland. This article is an open access article distributed under the terms and conditions of the Creative Commons Attribution license (<http://creativecommons.org/licenses/by/3.0/>).